

Validation of attenuation correction using transmission truncation compensation with a small field of view dedicated cardiac SPECT camera system

Gavin L. Noble, MD,^a Alan W. Ahlberg, MA,^b Aravind Rao Kokkiralala, MD,^b S. James Cullom, PhD,^c Timothy M. Bateman, MD,^{c,d,e} Giselle M. Cyr, BSN,^b Deborah M. Katten, BSN, MPH,^b Glenn D. Tadeo, CNMT,^b James A. Case, PhD,^c David M. O'Sullivan, PhD,^b and Gary V. Heller, MD, PhD^{b,f}

Background. Although attenuation correction (AC) has been successfully applied to large field of view (LFOV) cameras, applicability to small field of view (SFOV) cameras is a concern due to truncation. This study compared perfusion images between a LFOV and SFOV camera with truncation compensation, using the same AC solution.

Methods and Results. Seventy-eight clinically referred patients underwent rest-stress single-photon emission computed tomography (SPECT) using both a SFOV and LFOV camera in a randomized sequence. Blinded images were interpreted by a consensus of three experienced readers. The percentage of normal images for SFOV and LFOV was significantly higher with than without AC (72% vs 44% and 72% vs 49%, both $P < .001$). Interpretive agreement between cameras was better with than without AC ($\kappa = 0.736$ to 0.847 vs 0.545 to 0.774). Correlation for the summed stress score was higher with than without AC ($r^2 = 0.892$ vs 0.851 , both $P < 0.001$) while Bland Altman analysis demonstrated narrower limits with than without AC (4.0 to -4.3 vs 5.9 to -5.6).

Conclusion. Attenuation correction using truncation compensation with a SFOV camera yields similar results to a LFOV camera. The higher interpretive agreement between cameras after attenuation correction suggests that such images are preferable to non-attenuation-corrected images. (J Nucl Cardiol 2009;16:222-32.)

Key Words: Attenuation correction • truncation compensation • small field of view • SPECT myocardial perfusion imaging

From the Division of Cardiology,^a Bend Memorial Clinic, Bend, OR; The Nuclear Cardiology Laboratory of the Henry Low Heart Center, Division of Cardiology, and the Department of Research Administration,^b Hartford Hospital, Hartford, CT; Cardiovascular Imaging Technologies,^c Kansas City, MO; Mid America Heart Institute,^d and The University of Missouri-Kansas City,^e Kansas City, MO and The University of Connecticut School of Medicine,^f Farmington, CT.

This study was supported by an unrestricted educational medical grant from Philips Medical Systems, Milpitas, California.

Dr. Heller receives grant support and is on the speaking board of Philips Medical Systems. Drs. Bateman, Case, and Cullom receive software royalties from Philips Medical Systems for the attenuation correction and truncation compensation software.

Received for publication Feb 20, 2008; final revision accepted Oct 28, 2008.

Reprint requests: Gary V. Heller, MD, PhD, The University of Connecticut School of Medicine, Farmington, CT 06102; gheller@harthosp.org.

1071-3581/\$34.00

Copyright © 2008 by the American Society of Nuclear Cardiology. doi:10.1007/s12350-008-9022-4

INTRODUCTION

The value of single-photon emission computed tomography (SPECT) myocardial perfusion imaging (MPI) has been well documented for both diagnosis¹ and risk stratification.² Unfortunately, soft-tissue attenuation continues to reduce its effectiveness in determining the presence or absence of coronary artery disease (CAD), resulting in false positive findings that affect physician confidence and lead to unnecessary cardiac catheterizations.

To reduce the incidence of false positive studies, attenuation correction (AC) solutions have been developed with both radionuclide line source and computed tomography, resulting in higher diagnostic accuracy over MPI alone or with ECG-gated SPECT.³ Despite the benefits of AC, there are some technical challenges, one being truncation. Truncation occurs when a portion of

the body is outside the field of view of the detector, either because a patient is too large for the detector or when the detector field of view is small. The result is an artifact in the attenuation map potentially leading to inaccurate correction and misinterpretation.

Attenuation correction has been applied primarily to large field of view (LFOV) cameras in which truncation impact is minimized. However, as the field of nuclear cardiology moves toward smaller detectors that can rotate closer to the patients' chest and also require less space, truncation may become an issue for the continued success of AC. Recently, a method of truncation compensation for body habitus outside of the field of view for AC was developed, specifically for a small field of view (SFOV)-dedicated SPECT camera system.⁴ However, clinical data supporting the value of AC with this imaging technology are lacking. Therefore, the purpose of this study was to compare image quality, interpretive confidence, and myocardial perfusion SPECT characteristics between a LFOV camera, which has been well validated with AC, and a SFOV camera with truncation compensation software, using the same AC solution in patients with known or suspected CAD.

METHODS

Patient Population

Patients clinically referred for rest-stress Tc-99m sestamibi ECG-gated SPECT MPI within the Nuclear Cardiology Laboratory at Hartford Hospital, Hartford, Connecticut were screened for study participation. Eligibility criteria included an intermediate to high pretest likelihood⁵ or known CAD based on prior MI or coronary catheterization. Excluded from participation were lactating or pregnant females, patients exceeding table-weight limit of 350 pounds, those unable to complete all image acquisitions, or unwilling to sign informed consent. Body mass index (BMI) was calculated as weight (kg)/height (m)² (kg/m²) with patients classified as non-obese (BMI < 30) or obese (BMI ≥ 30) in accordance with the World Health Organization.⁶ This study was approved by and conducted within the guidelines established by the Institutional Review Board at Hartford Hospital.

Stress-Testing Protocols

Patients were instructed to fast ≥8 hours and to withhold β-blockers, caffeine-containing food, and drugs as well as oral dipyridamole for 24 to 48 hours before testing. Patients were scheduled for a specific stress modality according to the discretion of the referring physician, based upon perceived functional capacity. Vital signs and 12-lead ECG were monitored before, during, and after termination of testing and resolution of changes. Exercise and pharmacologic stress testing was performed utilizing standard protocols, techniques, and guidelines.^{7,8}

Image Acquisition Protocols and Parameters

Patients underwent rest and stress image acquisition with both a SFOV and a LFOV camera in a randomized sequence. The same sequence was followed for both the rest and stress image acquisitions. Rest images were acquired 45 to 60 minutes following administration of low-dose (10 to 15 mCi) or high-dose (30 to 45 mCi) Tc-99m sestamibi for patients in whom a same-day or two-day image acquisition protocol, respectively, was utilized. Stress images were acquired 15 to 60 minutes following high-dose (30 to 45 mCi) Tc-99m sestamibi administration.

Images with LFOV and SFOV were acquired on a Cardio 60 Vertex and Cardio MD fixed-90° dual head SPECT camera with a FOV dimension of 508 mm × 381 mm and 370 mm × 214 mm, respectively, each outfitted with commercially available AC hardware and software (VantagePro [Philips Medical Systems, Milpitas, CA] and ExSPECT II [Emory University, Atlanta, GA and Cardiovascular Imaging Technologies, Kansas City, MO]). With each camera, two gadolinium-153 scanning line sources, with activity of 250 mCi and line length of 640.4 mm for LFOV and 609.0 mm for SFOV were used permitting simultaneous acquisition of transmission and ECG-gated perfusion images. Data were collected in three individual photopeak energy windows: transmission, 100 keV ± 10%; Tc-99m emission, 140 keV ± 10%; and downscatter/scatter, 118 keV ± 6%. A total of 64 projections were obtained (25 to 40 seconds per projection) over a 180° right anterior oblique-left posterior oblique orbit. A matrix of 64 × 64, pixel size of 6.4 mm for both, and magnification of 38.0 cm² for LFOV was used. A zoom factor of 1.0 was used for SFOV. A reconstruction voxel dimension of 6.4 mm × 6.4 mm was used on LFOV and SFOV. A low-energy high-resolution (LEHR) collimator with similar resolutions and sensitivities was used for both FOV cameras. Circular rotation was employed and the patient was positioned close to the camera head to minimize truncation. No attempt was made to center the heart in the FOV for SFOV as opposed to centering the body in the LFOV as recommended per Philips Cardio60 Vertex Imaging parameters. The duration of both rest and stress image acquisition with the LFOV system was determined by the use of a scout image used for calculation of minimal required counts for the transmission scan. With the SFOV system, patient height and weight were entered and subsequently a time period per projection was calculated according to the BMI.

Image Processing

Non-attenuation-corrected (non-AC) and attenuation-corrected (AC) images were evaluated for quality control and reconstructed at a central laboratory (Cardiovascular Imaging Technologies, Kansas City, MO) into the standard three oblique views. The non-AC emission images were reconstructed via filtered backprojection with a Butterworth pre-filter (order, 5; critical frequency, 0.66 Nyquist) applied to the projections. For AC, the attenuation maps were reconstructed using a Bayesian algorithm approach after logarithmic inversion and

normalization to a reference scan.⁹ Thirty iterations were used with a uniform initial estimate. A Butterworth post-filter was then applied (order, 5; critical frequency, 0.66 Nyquist) on each transverse plane. The algorithm applies scatter correction to the emission photopeak via subtraction of the scaled data from the scatter window.⁹ The transmission projection data were also corrected for Tc-99m downscatter from simultaneous emission/transmission acquisition by using the same data but a different scaling value.⁹ Non-stationary, depth-dependent resolution compensation was achieved with a modified Wiener filter pre-processing approach (VantagePro/ExSPECT IITM) and maximum likelihood emission maximization (MLEM) reconstruction using an uniform initial estimate and 12 iterations of MLEM. The software includes automated transmission scan truncation quality control (ATSTQC) of the transmission map, an algorithm which measures truncation and transmission map count density for optimizing image quality.¹⁰ As detected by ATSTQC, "critical truncation" was compensated for as previously described⁴ and, in brief, the technique is based on an initial estimate of body symmetry in the transverse plane. The algorithm applies this conjugate projection information to estimate the reconstructed image values affected by truncation. Truncation compensation is performed automatically with no operator interaction or parameter selection.

Definition of Critical Truncation and Compensation with SFOV SPECT MPI

For image data acquired at rest and stress with the SFOV camera system, the presence and severity of truncation on both the left and right side of the patient was visually assessed on the transverse attenuation maps by an experienced imaging physicist using a 5-point scoring system (0 = no truncation, 1 = visible truncation mildly affecting soft tissue [$\leq 50\%$], 2 = visible truncation significantly affecting soft tissue [$>50\%$], 3 = visible truncation significantly impacting lung, and 4 = visible truncation significantly obliterating lung). A score ≥ 2 on the left or right side was considered critical truncation. Compensation of critical truncation was considered to have occurred when the score on both the left and right side was ≤ 1 after correction.

Image Interpretation

All images were interpreted without clinical information by a consensus of three experienced nuclear cardiologists. The rotating images were not displayed to prevent knowledge of the camera system. The SFOV and LFOV images for each patient were presented for interpretation in a randomized fashion but with time distance between the same patient studies to avoid memory of the initial image. Each image was assessed for both non-AC and AC perfusion at rest and stress using the ASNC/AHA/ACC standard 17-segment scoring model.¹¹ Electrocardiographic gating was not used to identify attenuation artifact. Image quality at rest and stress was subjectively rated by consensus as excellent, good, fair, poor, or uninterpretable. On rest and stress imaging, each segment was

scored for perfusion (0 = normal uptake, 1 = mild, 2 = moderate, 3 = severe reduction in uptake, 4 = absent uptake). Perfusion in each coronary vascular territory (left anterior descending [LAD], circumflex [Cx], and right coronary artery [RCA]) was assessed using traditional regional assignments and classified as normal or abnormal. If abnormal, perfusion was further classified as a reversible (complete or partial) defect or fixed defect. Reversibility in vascular territory perfusion was defined as a difference of a minimum 40% in count magnitude by visual estimation between stress and rest imaging. Interpretive confidence based on assessment of AC perfusion imaging with each FOV was categorized as: definitely normal, probably normal, equivocal, probably abnormal, or definitely abnormal. For each image, a summed stress score (SSS) and summed rest score (SRS) was calculated by adding the segment scores. A summed difference score (SDS) was calculated by subtracting the SRS from the SSS. Percent myocardial stress perfusion deficit was calculated by dividing the SDS by 68 (maximum score possible).

Statistical Analyses

All numerical values were expressed as mean \pm standard deviation or as proportions. Continuous variables were compared by use of paired *t* tests. Chi-square tests (Pearson or McNemar as appropriate) were used to examine differences in proportions. Agreement in image interpretation between camera systems was compared by means of percentages (simple agreement) and Cohen's kappa (κ) statistic¹² with κ values are classified as follows: <0.2 , poor; 0.21 to 0.4, fair; 0.41 to 0.6, moderate; 0.61 to 0.8, good; 0.81 to 1, excellent agreement. Clinically important agreement was defined *a priori* as a $\kappa > 0.5$.¹³ Agreement in summed perfusion scores was assessed by use of correlation coefficients (*r*), coefficients of determination (r^2), and Bland Altman analysis.¹⁴ The level for statistical significance was predetermined at $P < .05$, and all comparisons were two tailed. For statistical analysis, SPSS 15.0 (Chicago, IL, 2006) was used.

RESULTS

Patient Characteristics

Seventy-eight patients satisfied all criteria for study inclusion and subsequently completed all rest and stress image acquisitions with each camera system. Of these patients, the vast majority (92%) underwent a same-day rest-stress image acquisition protocol. Clinical characteristics of the patients are shown in Table 1. Forty percent of the patients had an intermediate to high pre-test likelihood of CAD while 60% had known CAD. The patients had a mean age of 60 ± 9 years and 32% were female. The mean BMI for the cohort was 30 ± 5 kg/m² (range: 18 to 49). Forty-eight percent of the patients underwent standard exercise stress, 18% underwent standard pharmacologic stress (dipyridamole in 12 patients and dobutamine in 2) while 34% underwent a

Table 1. Clinical characteristics of the study population (n = 78)

Age, years (range)	60 ± 9 (35-80)
BMI, kg/m ² (range)	30 ± 5 (18-49)
BMI < 30/≥30	42 (54%)/36 (46%)
Women/men	25 (32%)/53 (68%)
Diabetes Mellitus	34 (43%)
Smoking	43 (55%)
Hypertension	49 (63%)
Dyslipidemia	55 (70%)
CHF	5 (7%)
Prior MI	27 (34%)
Prior PCI or CABG	35 (45%)
β-blocker	43 (55%)
Calcium antagonist	11 (14%)
ACE inhibitor	26 (33%)

BMI, Body mass index; CHF, congestive heart failure; MI, myocardial infarction; PCI, percutaneous coronary intervention; CABG, coronary artery bypass grafting; ACE, angiotensin converting enzyme.

combined stress protocol of dipyridamole and symptom-limited exercise.

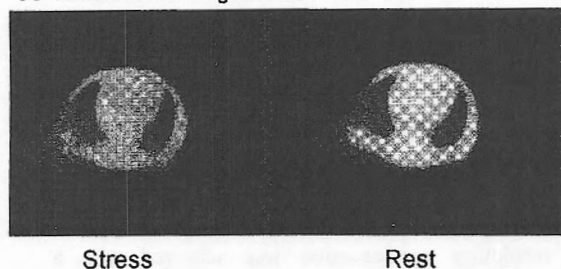
Incidence of Critical Truncation and Compensation with SFOV SPECT MPI

Data on the presence or absence of truncation on rest and stress SFOV transmission scans, both before and after compensation, were evaluated. Before compensation, 62 (79%) patients demonstrated right-sided truncation (60 on stress, 56 on rest, and 50 on both stress and rest scans), of which 27 (35%) were considered critical. Left-sided truncation before compensation was present in 3 (4%) patients (on stress in 3 and on rest in 1) and all were considered non-critical.

After compensation, 16 (21%) patients demonstrated right-sided truncation (12 on stress, 6 on rest, and 5 on both stress and rest scans), of which none was considered critical. Left-sided truncation after compensation was present in 1 patient (on both stress and rest scans), which was considered non-critical. Notably, the presence of truncation on transmission scans was significantly lower after than before compensation ($P < .001$). However, the presence of truncation, either before or after compensation, was not significantly associated with BMI ($P = NS$).

An example of truncation compensation is provided in Figure 1. The upper panel (A) represents the attenuation map of stress and rest without truncation compensation, demonstrating severe truncation on the patient's right side. The lower panel (B) represents the attenuation map after truncation compensation. The

A Truncation – Right-Sided



B Truncation Compensated

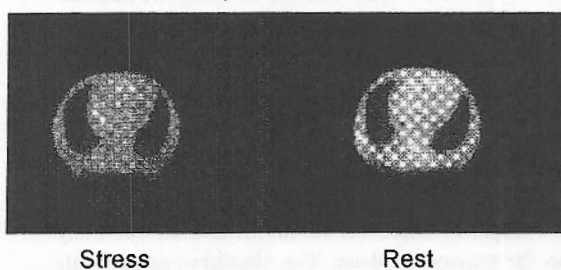


Figure 1. An example of truncation compensation in a patient. The upper panel A, represents the attenuation map of stress and rest without truncation compensation, while the lower panel B, represents the attenuation map after truncation compensation.

perfusion study in this 72-year-old male patient demonstrated a fixed inferior defect with moderate hypokinesis, consistent with the patient's history of prior myocardial infarction.

Image Quality

Of the 616 image quality assessments (data in one patient inadvertently was not collected), the majority with SFOV and LFOV were excellent or good on rest (92% and 79%, respectively) and stress (99% and 95%, respectively) SPECT. Fewer than 1% of images (6/616) were of poor quality (all were on rest SPECT) and none was considered to be uninterpretable. Attenuation correction had no significant effect on image quality with SFOV or LFOV (Table 2). However, a lower percentage of rest images were considered to be of excellent or good quality with AC than with non-AC, particularly with LFOV. Patients with a BMI ≥ 30 more frequently had fair or poor quality images compared to those with a BMI < 30, particularly on rest imaging with AC (29% vs 12%, respectively, $P = .009$).

Image Interpretation

Assessment of perfusion. With non-AC imaging, 54 (23%) of vascular territories were considered abnormal with each camera (17, 5, and 32 in LAD, Cx, and RCA distributions, respectively). The percentage of

Table 2. Image quality with SFOV and LFOV imaging without AC and with AC

	Non-AC			AC		
	SFOV	LFOV	P value	SFOV	LFOV	P value
Stress imaging						
Excellent or good	100% (77/77)	94.8% (73/77)	0.125	98.7% (76/77)	94.8% (73/77)	.25
Fair or poor	0% (0/77)	5.2% (4/77)		1.3% (1/77)	5.2% (4/77)	
Rest imaging						
Excellent or good	94.8% (73/77)	87% (67/77)	0.109	89.6% (69/77)	70.1% (54/77)	.003
Fair or poor	5.2% (4/77)	13% (10/77)		10.4% (8/77)	29.9% (23/77)	

SFOV, Small field of view; LFOV, large field of view; Non-AC, non-attenuation correction; AC, attenuation correction.

non-AC images in which one or more territories was considered abnormal was not significantly different between SFOV and LFOV (56% vs 51%, respectively, $P = NS$). These findings were independent of BMI ($P = NS$).

Of the 54 territories considered abnormal with non-AC imaging, 25 (46%) were considered normal with AC imaging with each camera. Of these, most were located in the RCA (21 and 20 with SFOV and LFOV, respectively) or LAD distribution (3 and 4 with SFOV and LFOV, respectively) and classified as fixed with non-AC (21 and 20 with SFOV and LFOV, respectively). With each camera, none of the territories with normal non-AC stress perfusion became abnormal with AC. Independent of camera, the percentage of AC images in which stress perfusion in each vascular territory was considered

normal was significantly higher than that of non-AC images (72% vs 44% and 72% vs 49% with SFOV and LFOV, respectively, both $P < .001$). These findings were independent of BMI (Figure 2).

Agreement between cameras for identification of non-AC stress perfusion abnormalities in specific vascular territories was moderate to good (92%, $\kappa = 0.774$ in LAD; 95%, $\kappa = 0.573$ in Cx; and 82%, $\kappa = 0.629$ in RCA), but considerably better (good to excellent) with AC (94%, $\kappa = 0.776$ in LAD; 97%, $\kappa = 0.736$ in Cx; and 96%, $\kappa = 0.847$ in RCA), particularly in the RCA territory. Similarly, there was moderate to good agreement between cameras in classifying non-AC images as normal, fixed defect(s), or reversible defect(s) and for the number of vascular territories with abnormal perfusion. However, with AC, agreement in these image

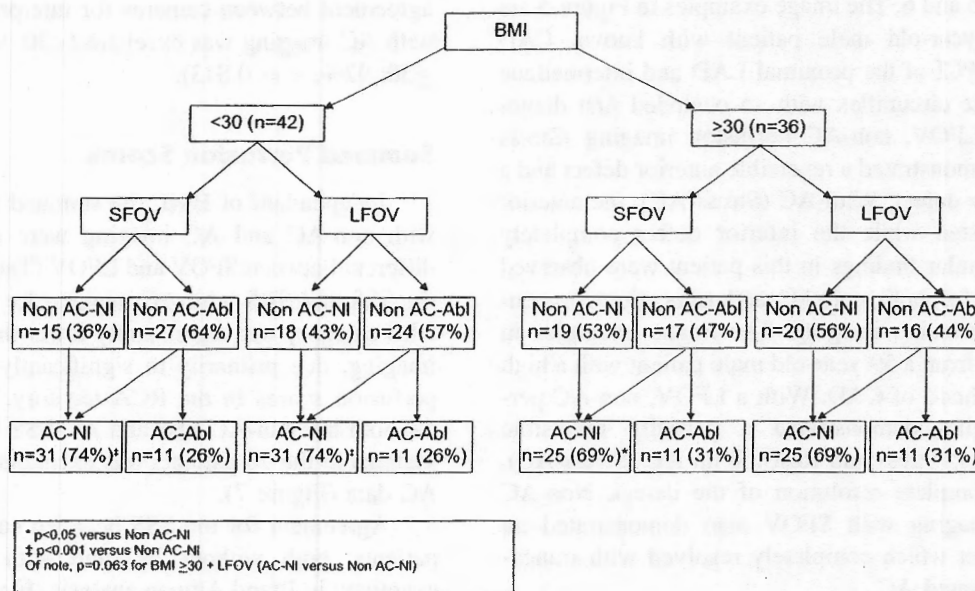


Figure 2. Percentage of images classified as having normal or abnormal stress perfusion without attenuation correction (non-AC) and with attenuation correction (AC) in relation to camera system (small field of view [SFOV] or large field of view [LFOV]) and body mass index ([BMI]: <30 or ≥30).

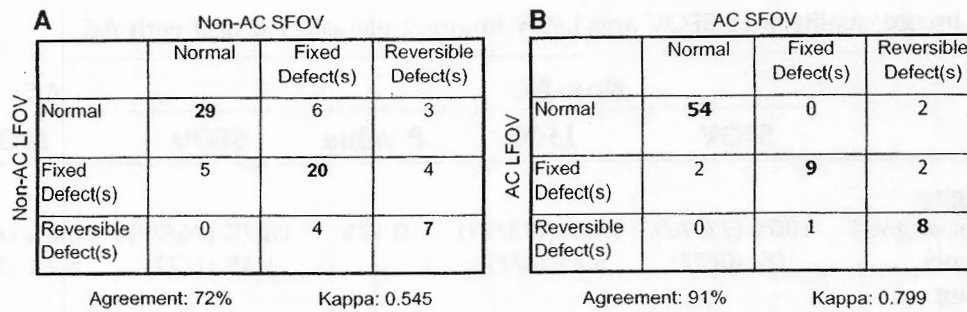


Figure 3. Agreement between small field of view (SFOV) and large field of view (LFOV) for classifying stress perfusion as normal vs fixed defect(s) vs reversible defect(s) on **A**, non-attenuation-corrected imaging (non-AC) and on **B**, attenuation-corrected imaging (AC).

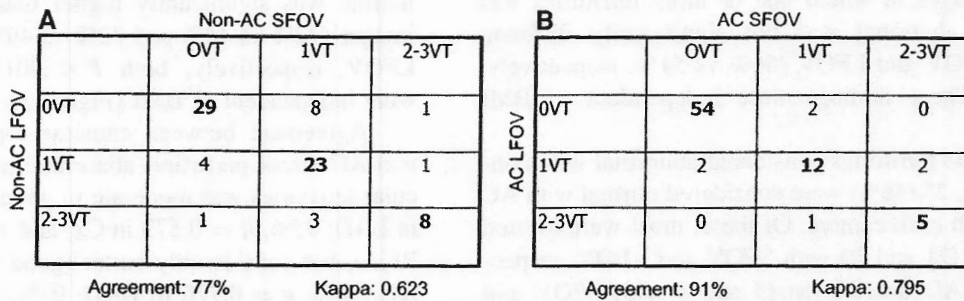


Figure 4. Agreement between small field of view (SFOV) and large field of view (LFOV) for classifying the number of vascular territories with abnormal stress perfusion on **A**, non-attenuation-corrected imaging (non-AC) and on **B**, attenuation-corrected imaging (AC).

classifications was excellent (Figures 3 and 4). Illustrating the value of AC with LFOV and SFOV cameras are Figures 5 and 6. The image examples in Figure 5 are from a 63-year-old male patient with known CAD (status-post PCI of the proximal LAD and intermediate branch of the circumflex with an occluded first diagonal). With LFOV, non-AC perfusion imaging (Stress and Rest) demonstrated a reversible anterior defect and a fixed inferior defect. With AC (Stress-AC), the anterior defect persisted while the inferior defect completely resolved. Similar findings in this patient were observed with SFOV for both non-AC and truncation-compensated AC perfusion imaging. The image examples in Figure 6 are from a 59-year-old male patient with a high pretest likelihood of CAD. With a LFOV, non-AC perfusion imaging demonstrated a partially reversible inferior defect (Stress and Rest). With AC (Stress-AC), there was complete resolution of the defect. Non-AC perfusion imaging with SFOV also demonstrated an inferior defect which completely resolved with truncation-compensated AC.

Interpretive confidence. Interpretive confidence for assessment of stress perfusion with AC imaging was very high (no equivocal categorizations) with 97% and 96% of studies being categorized as

definitely normal or definitely abnormal with SFOV and LFOV, respectively ($P = NS$). Independent of BMI, agreement between cameras for interpretive confidence with AC imaging was excellent (<30 : 91%, $\kappa = 0.761$; ≥ 30 : 92%, $\kappa = 0.813$).

Summed Perfusion Scores

Independent of BMI, the summed perfusion scores with non-AC and AC imaging were not significantly different between SFOV and LFOV (Table 3). However, the SSS and SRS with AC imaging for patients in each BMI category was significantly lower than with non-AC imaging, due primarily to significantly lower summed perfusion scores in the RCA territory. The correlation for both the non-AC SSS and AC SSS between camera systems in the 78 patients was excellent and better with AC data (Figure 7).

Agreement for the SSS between cameras in the 78 patients, both without AC and with AC, was also examined in Bland Altman analysis (Figure 8). With the non-AC SSS, this analysis showed a mean difference of 0.1 and upper and lower limits of 5.9 and -5.6, respectively. In 74 (95%) patients, the difference in the non-AC SSS between cameras ranged between 5.9 and

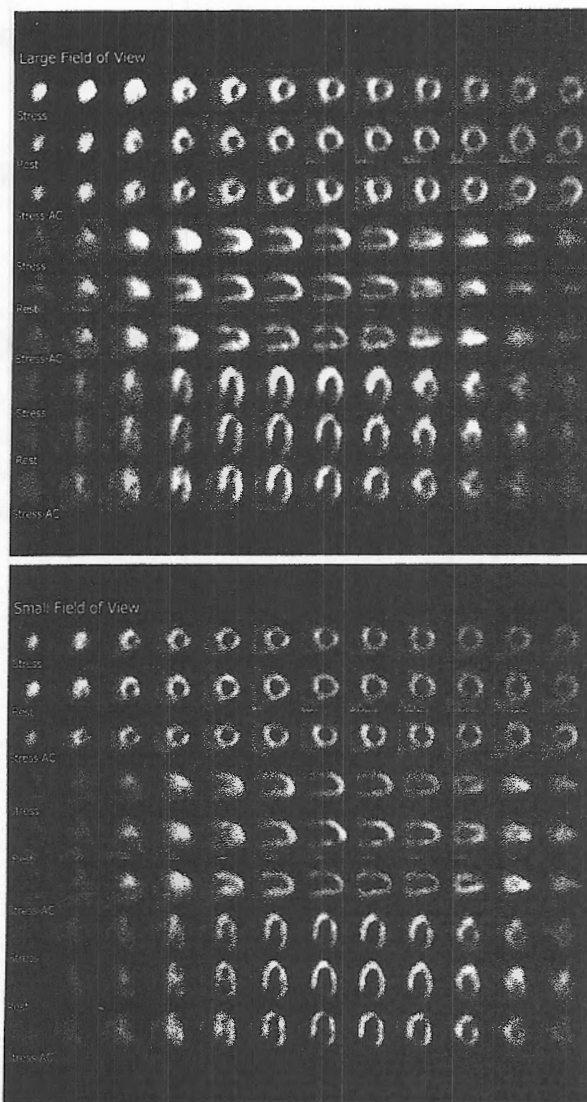


Figure 5. An example of LFOV and truncation-compensated-derived SFOV imaging in the same patient. With a large field of view camera, non-AC perfusion imaging (Stress and Rest) demonstrated a medium-sized reversible anterior and fixed inferior defect. Attenuation-corrected perfusion imaging (Stress-AC) demonstrated complete resolution of the inferior defect with persistence of the anterior defect. Similar findings with non-AC and AC perfusion imaging were observed with a SFOV camera.

–5.6. Of the four patients in whom the difference exceeded those limits, the non-AC SSS with one FOV in two (one in each BMI category) was substantially higher than that with the other FOV (difference of 13 and –12 with both patients demonstrating completely normal perfusion [non-AC SSS = 0] with one FOV). In contrast, Bland Altman analysis with the AC SSS showed a mean difference of –0.1 and upper and lower limits of 4.0 and –4.3, respectively. Notably, upper and lower limits for the SSS were narrower with AC than without

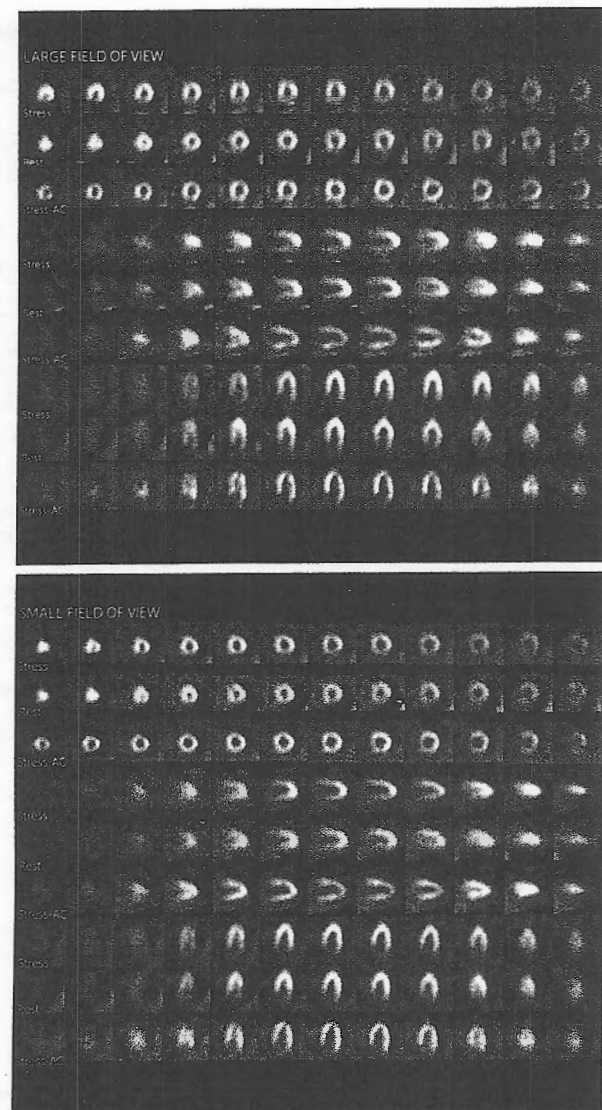


Figure 6. An example of LFOV and truncation-compensated-derived SFOV imaging in the same patient. With a LFOV camera, non-AC perfusion imaging (Stress and Rest) demonstrated a medium-sized partially reversible inferior defect. Attenuation-corrected perfusion imaging (Stress-AC) demonstrated completely normal perfusion. Non-AC perfusion imaging with a SFOV camera demonstrated a similar defect while AC perfusion imaging demonstrated completely normal perfusion, similar to that observed with a LFOV camera.

AC. In 71 (91%) patients, the difference in the AC SSS between cameras ranged between 4.0 and –4.3. Of the seven patients in whom the difference exceeded those limits, five (all with a BMI \geq 30) had concordant perfusion findings (definitely abnormal) of which three had an AC SSS $>$ 7 ($>$ 10% myocardial stress perfusion deficit) with each FOV. The remaining two patients (both with a BMI $<$ 30) had discordant perfusion findings (definitely normal and definitely abnormal with each FOV). In both cases, however, the perfusion

Table 3. Comparison of summed perfusion scores between SFOV and LFOV SPECT imaging without AC and with AC

	BMI < 30 (n = 42)		BMI ≥ 30 (n = 36)	
	Non-AC SFOV	Non-AC LFOV	Non-AC SFOV	Non-AC LFOV
SSS	4.2 ± 6.3	4.7 ± 7.1	5 ± 8.2	4.8 ± 8.1
SRS	3.3 ± 5.5	4 ± 6.7	3.7 ± 7.3	4.1 ± 7.9
SDS	0.9 ± 1.8	0.6 ± 1.7	1.3 ± 2.6	0.6 ± 1.6
	AC SFOV	AC LFOV	AC SFOV	AC LFOV
SSS	2.7 ± 5.9 [‡]	2.8 ± 6.3 [‡]	3.6 ± 7.1 [†]	3.2 ± 6.5 [†]
SRS	2.2 ± 5.5 [‡]	2.1 ± 5.1 [‡]	2.4 ± 6.2 [‡]	2.3 ± 5.6 [†]
SDS	0.5 ± 1.5*	0.7 ± 2.2	1.2 ± 2.6	0.9 ± 2.8

BMI, Body mass index; Non-AC, non-attenuation correction; AC, attenuation correction; SFOV, small field of view; LFOV, large field of view; SSS, summed stress score; SRS, summed rest score; SDS, summed difference score.

*P < .05 vs Non-AC.

[†] P < .01 vs Non-AC.

[‡] P < .001 vs Non-AC.

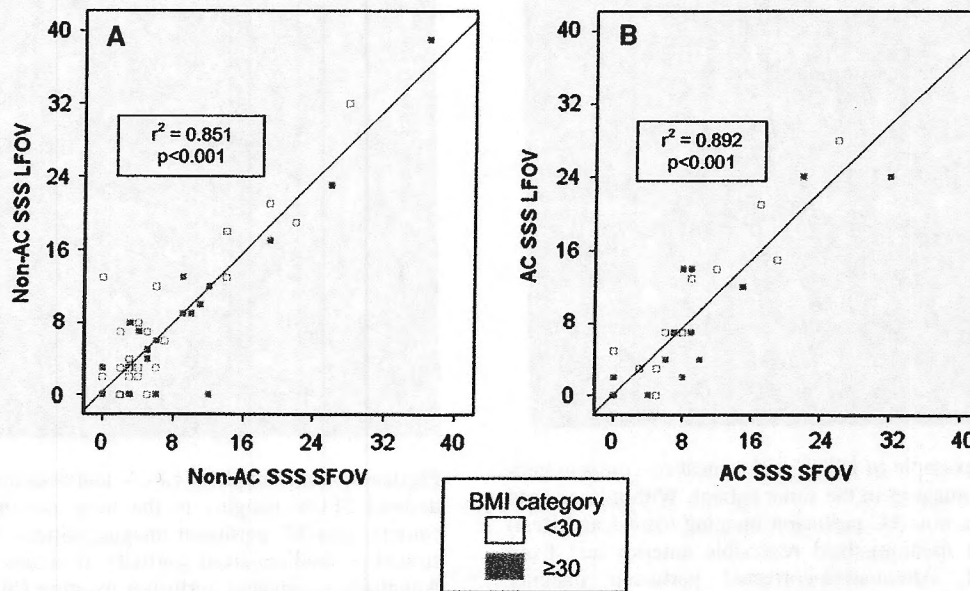


Figure 7. Correlation in the A, non-attenuation-corrected summed stress score (*non-AC SSS*) between small field of view (*SFOV*) and large field of view (*LFOV*) imaging in all patients (n = 78) and B, attenuation-corrected summed stress score (*AC SSS*) between small field of view (*SFOV*) and large field of view (*LFOV*) imaging in all patients (n = 78).

abnormality with one FOV was mild to moderate in severity and confined to a single vascular territory (AC SSS = 5 [$<10\%$ myocardial stress perfusion deficit]).

DISCUSSION

The purpose of this study was to evaluate the value of line-source AC with truncation compensation using a SFOV SPECT camera. The comparison, by design of a

randomized image acquisition protocol in the same patients, was with a LFOV SPECT camera with similar methodology but without truncation compensation, which has previously been validated for diagnostic accuracy.^{15,16} In a study cohort with either an intermediate to high pretest likelihood of or known CAD and wide range in BMI, application of AC to image data was found to have a similar impact with both camera systems resulting in a significant increase in the percentage of

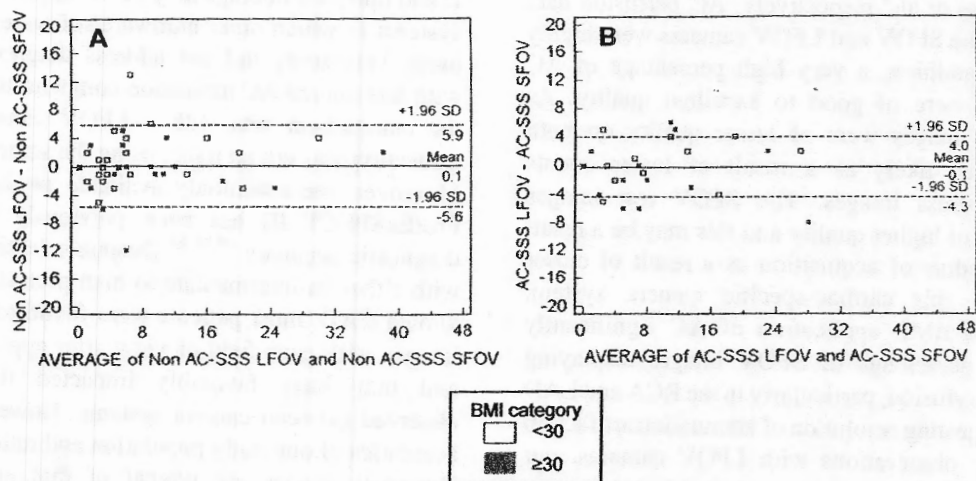


Figure 8. Bland Altman analysis comparing the **A**, non-attenuation-corrected summed stress score (*non-AC SSS*) between small field of view (*SFOV*) and large field of view (*LFOV*) imaging in all patients ($n = 78$) and **B**, attenuation-corrected summed stress score (*AC SSS*) between small field of view (*SFOV*) and large field of view (*LFOV*) imaging in all patients ($n = 78$).

SPECT images displaying normal stress perfusion. Our study demonstrates that this innovative AC technology with SFOV imaging provides data on stress perfusion that agree and correlate highly with LFOV imaging. Further, Bland Altman analysis of the summed stress score suggested better agreement between camera systems with AC. Hence, line-source AC using truncation compensation with SFOV SPECT MPI has clinical utility in the assessment of patients with known or suspected CAD and offers significant advantages over non-AC data.

Impact of Truncation Upon Line-Source AC

Whether truncation significantly impedes the effectiveness of AC in determining the presence or absence of CAD is still a source of debate. With early investigations, some studies^{17,18} suggested that accurate AC data could be obtained despite significant distortion of the attenuation map outside the full sampled region, particularly if right sided, while other reports^{19,20} concluded that severe truncation can negatively impact diagnostic accuracy. Nonetheless, the clinical utility of next generation hardware and software for AC with LFOV SPECT MPI has been validated and, thus, has become widely accepted within the nuclear cardiology community²¹ with the methodology now commercially available on several camera systems. This is primarily because truncation with such cameras is infrequent and when it occurs as right sided. Moreover, recent studies by Grossman et al¹⁵ and Thompson et al¹⁶ have demonstrated that AC on a LFOV SPECT camera without truncation compensation significantly increases specificity without a significant loss in sensitivity, further evidence supporting its clinical utility.

With the emergence of smaller cameras and detectors, truncation is an increased concern as it will occur more frequently with these systems and may negatively impact the accuracy of AC. Chen et al¹⁰ presented a quantitative evaluation of the impact of truncation on AC with SFOV SPECT MPI. The investigators determined that identification of left-side truncation as “critical truncation” with SFOV imaging is necessary since it will have a negative impact on AC. In addition, an “automated transmission scan truncation quality-control” (ATSTQC) algorithm was developed that can accurately detect critical truncation (sensitivity of 1.00 and specificity of 0.95) and assist clinicians in deciding whether to rely on AC data with interpretation of a particular imaging study.

When critical truncation is detected by ATSTQC, compensation is necessary for accurate AC data. Although various methods have been proposed to compensate for truncation,^{20,22-26} Case et al⁴ recently developed a truncation compensation technique specifically for SFOV cardiac SPECT systems with gadolinium-153 scanning line sources. To determine whether this technique provides accurate AC data with SFOV SPECT MPI, Chen et al¹⁰ applied truncation compensation to a simulated SFOV transmission scan with significant right and left side truncation which produced an attenuation map similar to that of the LFOV. That finding provided further evidence supporting the feasibility of attenuation correction with SFOV SPECT MPI.

This study provides the first data supporting the value of AC with the SFOV camera. In the current analysis, which utilized the ATSTQC algorithm and truncation compensation technique developed by Chen

et al¹⁰ and Case et al,⁴ respectively, AC perfusion data acquired with the SFOV and LFOV cameras were highly correlated. In addition, a very high percentage of AC SFOV images were of good to excellent quality. As expected, rest images were of lesser quality on both camera systems, likely as a result of lower counts compared to stress images. The SFOV rest images appeared to be of higher quality and this may be a result of a smaller radius of acquisition as a result of closer contouring on this cardiac-specific camera system. Independent of BMI, application of AC significantly increased the percentage of SFOV images displaying normal stress perfusion, particularly in the RCA and LAD territories, suggesting resolution of attenuation artifact. In contrast to the observations with LFOV cameras, our results with a SFOV camera demonstrated that truncation was frequent and more often right sided than left sided. In addition to the detectors being smaller, attention to patient positioning and an acquisition protocol that is designed to allow right side at the expense of left-side truncation are possible explanations for the difference in truncation between camera systems. Of potential importance, though, compensation of all critical truncation was demonstrated, validating its' clinical utility.

The better agreement of AC than non-AC data between camera systems as well as the high confidence with interpretation of SFOV images are findings of considerable importance. Our results indicate that variability with interpretation of myocardial perfusion between a LFOV and SFOV camera is lower when AC is applied, likely due to less artifact from soft tissue. In addition, interpretation of AC SFOV images will likely be more definitive than would occur with non-AC studies, which may favorably impact physician decisions in post-test patient management. Notably, high interpretive confidence with AC LFOV imaging was also observed in the current study and concurs with the previous findings of Thompson et al¹⁶ and Heller et al.²⁷ Thus, our study validates that line-source AC with truncation compensation is not only useful, but preferable to non-AC imaging.

Limitations

This study included patients with a wide range of body weights (114 to 295 lbs.), although results should not be applied to those weighing in excess of 300 lbs. (notably, the SFOV camera has a weight limit of 350 lbs.). Quantification was not used because the more common standard of practice of perfusion assessment is by visual assessment and with the exception of data from Grossman et al,¹⁵ quantification of AC perfusion has not been extensively validated. All images were acquired and processed by use of VantagePro/ExSPECT

II and thus, our findings may not be applicable to camera systems in which other hardware/software packages are used. This study did not address diagnostic accuracy with line-source AC truncation compensation. However, the comparison was with a LFOV camera in which truncation was not an issue, using the same AC solution. Moreover, the commonly available product (VantagePro/ExSPECT II) has been previously validated for diagnostic accuracy.^{15,16,27} Despite selection of patients with either an intermediate to high pretest likelihood or known CAD, most patients were found to have normal images with each field of view after application of AC and may have favorably impacted the agreement observed between camera systems. However, the characteristics of our study population and ratio of normal to abnormal images are typical of that encountered in clinical practice.

CONCLUSION

We conclude that using truncation compensation on a SFOV camera with line-source AC yields similar results to a LFOV camera in the same patients with a wide range of BMI. The greater concordance between SFOV and LFOV images after the application of truncation compensation and AC suggests that incorporating these technologies may be preferred to non-AC imaging.

Acknowledgments

The authors would like to acknowledge Sachin M. Navare, MD, for participation in image interpretation sessions; Hemal Kadakia, MD, Ryan Phillips, MS, Ivette Leka, BA, and Michele Masse, CNMT for assistance with data collection; and April Mann, CNMT, RTN, for technical assistance. Dr. Heller receives grant support and is on the speaking board of Philips Medical Systems. Dr.'s Bateman, Case and Cullom receive software royalties from Philips Medical Systems for the attenuation correction and truncation compensation software.

References

1. Underwood SR, Anagnostopoulos C, Cerqueira M, Ell PJ, Flint EJ, Harbinson M, et al. Myocardial perfusion scintigraphy: the evidence. A consensus conference organized by the British Cardiac Society, the British Nuclear Cardiology Society and the British Nuclear Medicine Society, endorsed by the Royal College of Radiologists. *Eur J Nucl Med Mol Imaging* 2003;31:261-91.
2. Shaw LJ, Iskandrian AE. Prognostic value of gated myocardial perfusion SPECT. *J Nucl Cardiol* 2004;11:171-85.
3. Singh B, Bateman TM, Case JA, Heller G. Attenuation artifact, attenuation correction, and the future of myocardial perfusion SPECT. *J Nucl Cardiol* 2007;14:153-64.
4. Case JA, Tsu BL, Cullom SJ, Bateman TM, Galt JR, Garcia EV. Correcting for transmission truncation artifacts using conjugate

- sonogram as posteriori information for transmission reconstruction [abstract]. IEEE Nuclear Science Symposium and Medical Imaging Conference, Portland, OR, Oct 19–25, 2003.
5. Diamond GA, Forrester JS. Analysis of probability as an aid in the clinical diagnosis of coronary-artery disease. *N Engl J Med* 1979;300:1350–8.
 6. Brown DB. The global epidemic of obesity. International Association for the Study of Obesity web site. From www.iotf.org.
 7. Henzlova MJ, Cerqueira MD, Mahmarian JJ, Yao SS. Quality Assurance Committee of the American Society of Nuclear Cardiology. Stress protocols and tracers. *J Nucl Cardiol* 2006;13:e80–90.
 8. Ignaszewski AP, McCormick LX, Heslip PG, McEwan AJ, Humen DP. Safety and clinical utility of combined intravenous dipyridamole/symptom-limited exercise stress test with thallium-201 imaging in patients with known or suspected coronary artery disease. *J Nucl Med* 1993;34:2053–61.
 9. Case JA, Hsu BL, Bateman TM, Cullom SJ. A Bayesian iterative transmission gradient reconstruction algorithm for cardiac SPECT attenuation correction. *J Nucl Cardiol* 2007;14:324–33.
 10. Chen J, Galt JR, Case JA, Ye J, Cullom SJ, Durbin MK, et al. Transmission scan truncation with small-field-of-view dedicated cardiac SPECT systems: Impact and automated quality control. *J Nucl Cardiol* 2005;12:567–73.
 11. Cerqueira MD, Weissman NJ, Dilsizian V, Jacobs AK, Kaul S, Laskey WK, et al. American Heart Association Writing Group on Myocardial Segmentation and Registration for Cardiac Imaging. Standardized myocardial segmentation and nomenclature for tomographic imaging of the heart: A statement for healthcare professionals from the Cardiac Imaging Committee of the Council on Clinical Cardiology of the American Heart Association. *Circulation* 2002;105:539–42.
 12. Cohen J. A coefficient of agreement for nominal scales. *Educ Psychol Measur* 1960;20:37–46.
 13. Fleiss JL. *Statistical methods for rates and proportions*. 2nd ed. New York: John Wiley and Sons; 1981. p. 222–3.
 14. Bland JM, Altman DG. Statistical methods for assessing agreement between two methods of clinical measurement. *Lancet* 1986;1(8476):307–10.
 15. Grossman GB, Garcia EV, Bateman TM, et al. Quantitative tc-99 sestamibi attenuation-corrected SPECT: Development and multi-center trial validation of myocardial perfusion stress gender-independent normal database in an obese population. *J Nucl Cardiol* 2004;11:263–72.
 16. Thompson RC, Heller GV, Johnson LL, Case JA, Cullom SJ, Garcia EV, et al. Value of attenuation correction on ECG-gated SPECT myocardial perfusion imaging related to body mass index. *J Nucl Cardiol* 2005;12:195–202.
 17. Gullberg GT, Morgan HT, Zeng GL, Christian PE, Di Bella EVR, Tung C-H, et al. The design and performance of a simultaneous transmission and emission tomography system. *IEEE Trans Nucl Sci* 1998;45:1676–98.
 18. Manglos SH, Gagne GM, Bassano DA. Quantitative analysis of image truncation in focal-beam CT. *Phys Med Biol* 1993;38:1443–57.
 19. Gregoriou GK, Tsui BMW, Gullberg GT. Evaluation of the effect of truncation in fan-beam cardiac SPECT using an observer study [abstract]. *J Nucl Med* 1994;35:p4–5.
 20. Gregoriou GK, Tsui BMW, Gullberg GT. Effect of truncated projections on defect detection in attenuation-compensated fan-beam cardiac SPECT. *J Nucl Med* 1998;39:166–75.
 21. Hendel RC, Corbett JR, Cullom SJ, DePuey EG, Garcia EV, Bateman TM. The value and practice of attenuation correction for myocardial perfusion SPECT imaging: a joint position statement from the American Society of Nuclear Cardiology and the Society of Nuclear Medicine. *J Nucl Cardiol* 2002;9:135–43.
 22. Laurette I, Clackdoyle R, Welch A, Natterer F, Gullberg GT. Comparison of three applications of ConTraSPECT. *IEEE Trans Nucl Sci* 1999;46:2146–53.
 23. Clackdoyle R, Noo F, Guo J, Roberts J. A quantitative reconstruction from truncated projections in classical tomography. *IEEE Trans Nucl Sci* 2004;51:2570–8.
 24. Clackdoyle R, Noo F. A large class of inversion formulas for the 2D radon transform of functions of compact support. *Inv Prob* 2004;20:1281–91.
 25. Noo F, Clackdoyle R, Pack JD. A two-step Hilbert transform method for 2D image reconstruction. *Phys Med Biol* 2004;49:3903–23.
 26. Zou Y, Pan X, Sidky EY. Imaging reconstruction in regions-of-interest from truncated projections in a reduced fan-beam scan. *Phys Med Biol* 2005;50:13–28.
 27. Heller GV, Bateman TM, Johnson LL, Cullom SJ, Case JA, Galt JR, et al. Clinical value of attenuation correction in stress-only Tc-99m sestamibi SPECT imaging. *J Nucl Cardiol* 2004;11:273–81.

